Evidence of Dynamical Jahn−Teller Effect on Triphenylene Radical Cation: Resonance Raman Spectrum and ab Initio Quantum-Chemical Calculations

Tamas Keszthelyi,[†] Gurusamy Balakrishnan, and Robert Wilbrandt*

Condensed Matter Physics and Chemistry Department, FYS-313, Risø National Laboratory, DK-4000 Roskilde, Denmark

W. Atom Yee

Department of Chemistry, Santa Clara University, Santa Clara, California 95053

Fabrizia Negri*

Dipartimento di Chimica "G. Ciamician", Via F. Selmi, 2, I-40126 Bologna, Italy

Received: February 18, 2000; In Final Form: June 19, 2000

We report resonance Raman spectrum of the triphenylene radical cation generated by γ-irradiation in a Freon glass at 77 K. Raman spectra were obtained using excitation in resonance with the strong cation absorption band near 400 nm. Ab initio calculations (Hartree−Fock, B-LYP, and B3-LYP, all with 6-31G basis set) were performed to obtain the equilibrium structures and vibrational force fields of triphenylene neutral and radical cation species. In addition, semiempirical calculations were carried out to identify the state in resonance with the excitation light and to simulate the vibronic structure of the resonance Raman spectrum. From these experimental and theoretical results, it is concluded that the bands observed in the resonance Raman spectrum of the radical cation contain the signatures of the Jahn−Teller effect on the cation which, similarly to benzene cation, is dynamical in nature.

1. Introduction

In recent years there has been considerable interest in triphenylene-based discotic (columnar) liquid crystalline materials because of their potential in electronic applications. Discogenic molecules contain a planar, rigid, usually aromatic core with four, six, or eight lipophilic substituents. In the mesophase, these disklike molecules aggregate by stacking into columns, allowing for close face-to-face contact of π-orbitals[1] such that quasi-one-dimensional energy or charge migration can take place. The columns are arrayed in a two-dimensional lattice in which the intercolumn distance is 20−40 Å. High charge carrier mobilities ($\sim 10^{-5}$ m^2 V^{-1} s^{-1}) for hexakis(*n*-hexylsulfanyl)-triphenylene have been reported,[2] and photoconductivity has been demonstrated also for the mesophase of hexakis(pentyloxy)triphenylene.[3,4] Photophysical properties of hexakis(alkyloxy)triphenylenes have been studied extensively.[5−8] We have recently reported on the photophysical properties of hexakis(*n*-hexylsulfanyl)triphenylene, hexakis(*n*-hexylsulfonyl)triphenylene, the unsubstituted triphenylene (see Figure 1) and hexakis(*n*-hexyloxy)triphenylene.[9] The goal of that work was to obtain information about the effect of various substituents on the triphenylene (TPH) core system. It was found that alkylsulfanyl substituents interact more strongly with the core than alkylsulfonyl and alkyloxy substituents. To better understand the photophysics of the parent system, we have also recently investigated experimentally and theoretically the unusual TPH phosphorescence spectrum.[10]

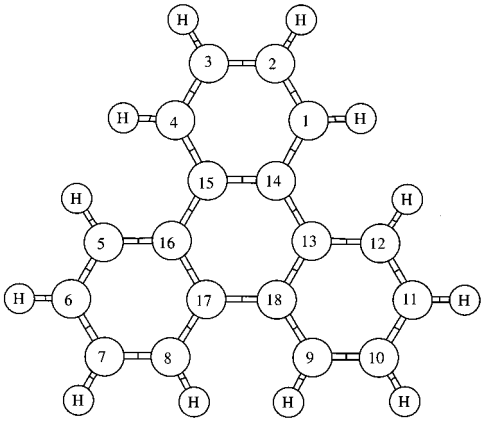

Figure 1. Triphenylene structure and the numbering system used to describe calculated geometrical parameters.

Doping of hexakis(*n*-hexyloxy)TPH with Lewis acids such as $AlCl_3$ converts the liquid crystalline material from an insulator into a semiconductor. Furthermore, it has been shown in this system that the oxidized form of the discotic liquid crystal is one in which a single charge is located on a single molecule, i.e., the radical cation of the substituted TPH.[11] Because this species is important to electronic conduction, it is interesting to know the structure of the radical cation and also to know the effect of various substituents on its energy. In recent years, we have conducted structural studies of many radical cation species using resonance Raman (RR) spectroscopy and molecular orbital calculations. These systems include 1,3-butadiene,[12−14] bithiophene,[15] and amines.[16−19] The present work applies our methodology to characterize the radical cation of the parent unsub-

* Authors to whom correspondence should be addressed.
[†] Present address: Department of Chemistry, Århus University, DK-8000 Århus C, Denmark.

10.1021/jp000672b CCC: $19.00
Published on Web 09/14/2000

stituted TPH. In this paper, we report RR spectra of TPH radical cation generated by γ-irradiation in a low-temperature Freon matrix. Ab initio calculations are carried out to obtain equilibrium structures and vibrational force fields of the radical cation along with the neutral species. Following the approach tested in our recent studies on the ions of aromatic and conjugated molecules,[20,21] the ab initio computed vibrational force fields are combined with semiempirical estimates of geometry change upon electronic excitation to simulate the vibronic activity in the RR spectra. Recent calculations on TPH radical cation[22−24] predict it to have C_{2v} symmetry, the lowering of the symmetry being attributed to the Jahn−Teller (JT) effect. To our knowledge, this is the first experimental evidence to show the existence of such effect on the radical cation of TPH.

2. Experimental and Theoretical Methods

Materials. TPH (Aldrich) was purified by column chromatography and by sublimation to remove impurities which fluoresce when excited at 400 nm. Biphenyl (Aldrich) was recrystallized twice from CH_3CN. The Freon solvents $CFCl_3$ and $BrCF_2-CF_2Br$ (Aldrich) were dried over molecular sieves. Acetonitrile (Lab-Scan Supergradient, HPLC grade), 1,4-diazabicyclo[2.2.2]octane (DABCO, Aldrich), and fumaronitrile (Aldrich) were used without further purification.

Generation and Detection of the Radical Cations. The apparatus and procedure used to obtain the RR spectra of TPH radical cation are described in detail elsewhere.[12−19]

Low-temperature experiments in the Freon matrix used 1:1 (v/v) mixtures of the above Freons. For measuring the electronic absorption spectrum, a 1.5×10^{-2} M TPH solution in a 7×7 mm^2 quartz cell was cooled to 77 K, forming a transparent glass. It was then irradiated with a dose of 0.1 MRad by ^{60}Co γ-rays. For measuring Raman spectra, 3×10^{-3} M TPH concentration, 0.3 MRad dose, and a 10 mm inner diameter cylindrical cell were used. After irradiation, samples were transferred to an Oxford Instruments DN1704 liquid nitrogen cryostat to perform optical measurements. Electronic absorption spectra of the radical cation were measured on a Perkin-Elmer Lambda 5 UV/vis spectrophotometer. Raman spectra at 77 K were recorded by excitation at 405 nm (5 mJ/pulse, 5 ns, 10 Hz) from a Continuum Sunlite optical parametric oscillator (OPO) laser. The OPO was pumped by 355 nm from a Nd:YAG (continuum Powerlite, PL9010). During these experiments, the cells were rotated at 8 rpm in the cryostat. The scattered light was collected in a backscattering geometry, and analyzed with a Jobin-Yvon T64000 spectrometer used in triple subtractive mode. A polarization scrambler was placed in front of the spectrometer, and a slit width of 0.2 mm was used. The spectral resolution at this wavelength is ca. 8−9 cm^{-1}.

We also carried out experiments at room temperature (not shown in the paper). In these experiments, radical cations were produced via photoinduced electron transfer between excited TPH (0.24 mM) and the electron acceptor fumaronitrile (24 mM) in oxygen-saturated acetonitrile solution. A 248 nm pulse from an excimer laser (Lambda Physik LPX200I, 6 mJ/pulse, 10 Hz KrF excimer laser) was used as the pump, and a 400 nm pulse (4 mJ/pulse) from the OPO laser was used as the probe. These resonance Raman spectra were in qualitative agreement with those observed from the Freon matrix. However, experiments were difficult because of very weak scattering and buildup of fluorescing photoproducts.

Raman spectra were detected by a Spectroscopy Instruments OSMA IRY-700 gated optical multichannel analyzer (OMA) having 700 active channels. To span the 400−1600 cm^{-1} spectral range, two spectra each spanning 1000 cm^{-1} were recorded and combined. The final TPH radical cation spectra were obtained by subtraction of probe-only spectra from pump−probe spectra to eliminate solvent and neutral TPH Raman bands.

Computational Methods and Modeling of the Resonance Raman Activity. Ab initio molecular orbital calculations were performed at three different levels of theory: Hartree−Fock (HF); B-LYP, a pure density functional theory (DFT) method that uses the Becke exchange functional[25] and the Lee, Yang and Parr correlation functional;[26] and B3-LYP, the Becke's three-parameter hybrid method[27] that uses the same LYP correlation functional. All three were used with the standard 6-31G basis set, as contained in the Gaussian 98 suite of programs.[28] The radical cation calculations were carried out with the restricted open shell approach at the HF level of theory (ROHF) and the unrestricted approach for the DFT calculations (UB-LYP, UB3-LYP). Vibrational frequencies were calculated at the critical points whose structures were optimized using Gaussian 98.

Electronic states of TPH radical cation were computed by employing a modified version[29,30] of the quantum consistent force field for π electrons (QCFF/PI) Hamiltonian[31] which includes a configuration interaction (CI) algorithm for the calculation of electronic states of any spin multiplicity.[32] In recent years, we have used this method to predict successfully ground and excited states of several radical ions and molecules in high spin states.[20,21,33,34]

The RR spectrum of TPH radical cation was simulated by considering that the Franck−Condon (FC) mechanism (*A* term in Albrecht's notation)[35] is the main source of intensity when the excitation wavelength is in resonance with a strong electronic transition. In this case, the vibronic structure is dominated by the activity of totally symmetric (TS) modes and can be modeled by assuming the harmonic approximation and by computing, for each *i*th TS mode, the displacement parameter B_i, relative to the strong resonant $D_0 \rightarrow D_n$ transition. The displacement parameter B_i is defined as

$$B_i = 0.172\omega_i^{1/2}(X_{D_n} - X_{D_0})M^{1/2}L_i^{D_0} \qquad (1)$$

where X_{D_n} and X_{D_0} are the Cartesian coordinate vectors which define the equilibrium structures of the two electronic states involved in the transition. M is the $3N \times 3N$ diagonal matrix of atomic masses, $L_i^{D_0}$ is the $3N$ vector describing the normal coordinate $Q_i^{D_0}$ in terms of mass-weighted Cartesian coordinates, and ω_i is the associated vibrational frequency (cm^{-1}). Under the assumption of resonance with the 0−0 band of the $D_0 \rightarrow D_n$ transition, the activity of each TS mode is related to the B_i parameter through the γ_i parameter

$$I_i \propto \gamma = {}^1/_2 B_i^2 \qquad (2)$$

In summary, to simulate the RR spectrum of TPH cation we need to identify the states responsible for the strong intensity in the absorption spectrum and we must calculate ground and excited state equilibrium geometries along with ground state vibrational normal coordinates and frequencies.

3. Results

Freon Matrix Experiments. We measured the electronic absorption spectrum of TPH cation in the Freon matrix in the region 350−600 nm (not shown), and it is identical to the spectrum obtained by Shida.[36] A structured strong absorption

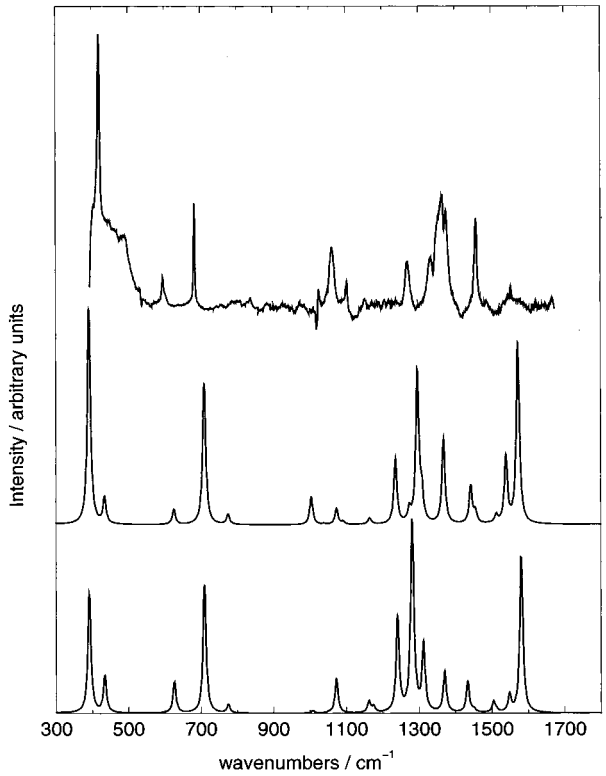

Figure 2. Comparison between experimental and calculated resonance Raman spectrum of TPH cation. (top) Resonance Raman spectrum obtained with 405 nm excitation of triphenylene radical cation generated by γ-irradiation in a Freon matrix at 77 K. (center) Simulated resonance Raman spectrum of TPH cation for the $D_0' \rightarrow D_6'$ transition, from QCFF/PI calculations. (bottom) Spectrum simulated for the $D_0 \rightarrow D_6$ transition, from QCFF/PI calculations (see the discussion in the text).

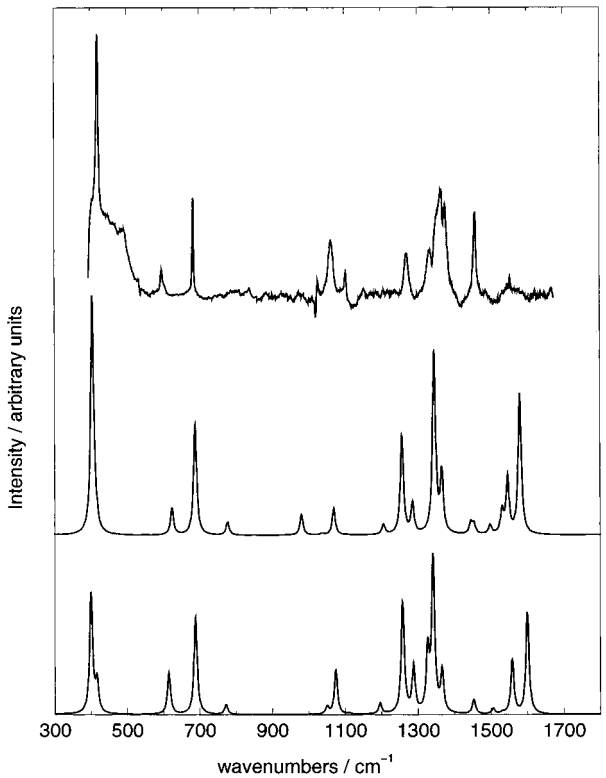

Figure 3. Comparison between experimental and calculated resonance Raman spectrum of TPH cation. (top) Resonance Raman spectrum obtained with 405 nm excitation of triphenylene radical cation generated by γ-irradiation in a Freon matrix at 77 K. (center) Simulated resonance Raman spectrum of TPH cation for the $D_0' \rightarrow D_6'$ transition, from QCFF/PI geometry changes and B-LYP/6-31G vibrational normal coordinates and frequencies. (bottom) Spectrum simulated for the $D_0 \rightarrow D_6$ transition, from QCFF/PI geometry changes and B-LYP/6-31G vibrational normal coordinates and frequencies (see the discussion in the text).

band occurs in the blue region of the spectrum with a maximum at 405 nm, and this wavelength was chosen for excitation in the RR measurements. The upper trace in Figures2 and 3 shows the resulting RR spectrum in the region 400−1600 cm^{-1} of TPH radical cation at 77 K in the Freon matrix.

The possibility of formation of aggregates was not a major concern given the low concentration employed to record the RR spectrum, and we have not seen evidence for dimers or higher aggregates. Similarly, there was no evidence for distortion in the low-temperature matrix, a fact supported by the agreement between calculations and experimental data (see below).

There are 12 bands identified in this spectrum: 11 of them can be assigned as fundamentals and one as an overtone (vide infra).

Molecular Structure of Neutral TPH. We carried out geometry optimizations and vibrational frequency calculations for neutral TPH and its radical cation species using the HF, B-LYP, and B3-LYP methods and the 6-31G basis set in order to compare the calculated geometrical parameters (bond lengths and bond angles) and vibrational frequencies for the two species. The B3-LYP method was chosen also to allow comparison of our results to those of recent calculations on triphenylene radical cation by Ling and Lifshitz[22] (B3-LYP/3-21G) and by Langhoff[23] (B3-LYP/4-31G).

For neutral TPH, the equilibrium structure obtained from the calculations belongs, as expected, to D_{3h} symmetry. Table 1 shows the experimental and calculated geometrical parameters for the neutral species. For comparison, the equilibrium structure of TPH computed[10] with QCFF/PI is also reported. The experimental values are data taken from Schettino's article[37] and are derived from X-ray data.[38] Bond lengths and bond angles in the table are given according to the numbering scheme in Figure 1. Comparison of the experimental data with calculated bond lengths shows that the HF method generally underestimates bond lengths, while both DFT methods overestimate bond lengths. The mean absolute differences between experimental and calculated values for the three methods, weighted for the number of bonds, are 0.010, 0.018, and 0.007 Å for HF, B-LYP, and B3-LYP, respectively. All calculated bond angles fit well to experimental values.

Molecular Structure of TPH Radical Cation. Since the highest two occupied molecular orbitals of neutral TPH correspond to a degenerate pair in D_{3h} symmetry, there are two JT distorted structures for the cation, similarly to benzene cation. Both belong to C_{2v} symmetry and recent DFT calculations have indicated a very small energy difference between the two.[24]

The two C_{2v} structures are, indeed, strictly related to the shape of the two possible singly occupied molecular orbitals (SOMOs).[24] In previous work on polyenes and bithiophene, we also found that bond length changes upon ionization are associated with nodal properties of the HOMOs of the neutral species.[39] Removal of an electron from this orbital leads to lengthening along bonds which have bonding interaction between atoms, and shortening along bonds which have antibonding interaction between atoms. The two SOMOs of TPH cation belong to two different symmetry representations of the C_{2v} point group: A_2 and B_1. Thus, the two JT distorted structures correspond to two different electronic states of A_2 and B_1 symmetry. The determination of the most stable structure is a delicate problem. Ab

TABLE 1: Calculated Geometrical Parameters for Neutral and Cationic Triphenylene in D_{3h} Symmetry[a]

	S_0					D_0			
	expt[b]	QCFF/PI	HF	B-LYP	B3-LYP	QCFF/PI	ROHF	UB-LYP	UB3-LYP
r(1−2)	1.378	1.3958	1.3723	1.3975	1.3869	1.3944	1.3710	1.3999	1.3887
r(2−3)	1.401	1.4062	1.3942	1.4142	1.4042	1.4072	1.4028	1.4184	1.4091
r(1−14)	1.416	1.4262	1.4076	1.4266	1.4161	1.4287	1.4096	1.4287	1.4183
r(14−15)	1.416	1.4348	1.4040	1.4393	1.4252	1.4505	1.4284	1.4552	1.4432
r(15−16)	1.447	1.4828	1.4696	1.4767	1.4688	1.4653	1.4491	1.4627	1.4524
α(1,2,3)	119.6	120.0	119.62	119.66	119.65	120.01	120.02	119.87	119.90
α(2,1,14)	122.0	121.4	121.80	121.91	121.86	121.77	121.46	121.76	121.68
α(1,14,15)	118.4	118.6	118.58	118.43	118.49	118.20	118.52	118.37	118.42
α(13,14,15)	120.0	120.0	120.00	120.00	120.00	120.00	120.00	120.00	120.00

[a] Bond lengths in Å, bond angles in degrees. [b] From ref 37, derived from X-ray data of ref 38.

TABLE 2: Calculated Geometrical Parameters for the Two C_{2v} Structures of Triphenylene Radical Cation[a]

	QCFF/PI		ROHF		UB-LYP		UB3-LYP	
	A_2	B_1	A_2	B_1	A_2	B_1	A_2	B_1
r(2−3)	1.3938	1.4248	1.3848	1.4295	1.4042	1.4325	1.3938	1.4252
r(14−15)	1.4456	1.4672	1.4067	1.4557	1.4363	1.4748	1.4244	1.4635
r(17−18)	1.4338	1.4860	1.4146	1.4760	1.4458	1.4806	1.4327	1.4727
r(3−4)	1.4044	1.3818	1.3832	1.3538	1.4108	1.3894	1.4003	1.3767
r(4−15)	1.4221	1.4363	1.3972	1.4253	1.4255	1.4325	1.4127	1.4244
r(15−16)	1.4742	1.4479	1.4664	1.4357	1.4710	1.4535	1.4619	1.4422
r(16−17)	1.4624	1.4515	1.4397	1.4166	1.4649	1.4460	1.4534	1.4338
r(8−17)	1.4487	1.4112	1.4361	1.3899	1.4435	1.4142	1.4351	1.4021
r(5−16)	1.4160	1.4398	1.3939	1.4137	1.4185	1.4403	1.4077	1.4292
r(5−6)	1.3963	1.3929	1.3795	1.3742	1.4017	1.3970	1.3752	1.3866
r(6−7)	1.4146	1.3993	1.4086	1.3892	1.4259	1.4115	1.4170	1.4013
r(7−8)	1.3810	1.4068	1.3567	1.3871	1.3869	1.4133	1.3912	1.4029
α(2,3,4)	120.09	120.19	119.75	120.43	119.56	120.19	119.60	120.23
α(3,4,15)	121.43	121.84	121.33	121.42	121.94	121.57	121.80	121.52
α(4,15,14)	118.48	117.97	118.91	118.15	118.49	118.23	118.60	118.24
α(14,15,16)	119.90	120.10	119.79	119.94	120.14	119.89	120.08	119.92
α(15,16,17)	119.67	120.32	120.00	120.14	119.80	120.18	119.83	120.18
α(16,17,18)	120.43	119.59	120.21	119.91	120.06	119.93	120.09	119.90
α(8,17,16)	117.58	118.91	118.37	118.57	118.46	118.35	118.52	118.35
α(5,16,17)	118.60	117.79	118.22	118.83	118.15	118.62	118.15	118.67
α(6,5,16)	121.82	121.47	121.55	121.51	121.70	121.78	121.66	121.70
α(5,6,7)	120.10	120.27	120.99	119.22	120.46	119.29	120.55	119.27
α(6,7,8)	120.28	120.01	119.23	120.45	119.63	120.17	119.58	120.22
α(7,8,17)	121.62	121.55	121.65	121.43	121.59	121.89	121.54	121.79

[a] Bond lengths in Å, bond angles in degrees.

TABLE 3: Changes in Calculated Bond Lengths, *r*(radical cation) − *r*(neutral), for the two C_{2v} Structures of Triphenylene Cation (Å)

	QCFF/PI		ROHF		UB-LYP		UB3-LYP	
bonds	A_2	B_1	A_2	B_1	A_2	B_1	A_2	B_1
r(2−3)	−0.0124	0.0186	−0.0094	0.0353	−0.0100	0.0183	−0.0104	0.0210
r(14−15)	0.0108	0.0324	0.0027	0.0517	−0.0030	0.0355	−0.0008	0.0383
r(17−18)	−0.0490	0.0032	−0.0550	0.0064	−0.0309	0.0039	−0.0361	0.0039
r(3−4)	0.0086	−0.0140	0.0109	−0.0185	0.0133	−0.0081	0.0134	−0.0102
r(4−15)	−0.0041	0.0101	−0.0104	0.0177	−0.0011	0.0059	−0.0034	0.0083
r(15−16)	−0.0086	−0.0349	−0.0032	−0.0339	−0.0057	−0.0232	−0.0069	−0.0266
r(16−17)	0.0276	0.0167	0.0357	0.0126	0.0256	0.0067	0.0282	0.0086
r(8−17)	0.0225	−0.0150	0.0285	−0.0177	0.0169	−0.0124	0.0190	−0.0140
r(5−16)	−0.0102	0.0136	−0.0137	0.0061	−0.0081	0.0137	−0.0084	0.0131
r(5−6)	0.0005	−0.0029	0.0072	0.0019	0.0042	−0.0005	−0.0117	−0.0003
r(6−7)	0.0084	−0.0069	0.0144	−0.0050	0.0117	−0.0027	0.0128	−0.0029
r(7−8)	−0.0148	0.0110	−0.0156	0.0148	−0.0106	0.0158	0.0041	0.0160

initio ROHF and semiempirical QCFF/PI predict the A_2 state as the global minimum, while DFT calculations point to a lowest energy structure of B_1 symmetry and predict the A_2 state to be a saddle point (see below). A summary of calculated geometrical parameters for the two C_{2v} structures of TPH radical cation is collected in Table 2. Table 3 shows the changes in bond lengths calculated by the various theoretical methods for the two C_{2v} structures of the radical cation. The positive values indicate bond lengthening, and negative values indicate bond shortening, upon ionization of TPH. It is seen that the predicted bond length changes for the two C_{2v} structures of TPH cation do not depend strongly on the level of theory employed, in accord with the notion that the shape of the SOMO determines the structure of the A_2 and B_1 states. Calculations were also carried out to optimize the structure of TPH cation in D_{3h} symmetry. A summary of the geometrical parameters of the D_{3h} optimized structures is presented in the last four columns of Table 1. It is seen that the larger changes occurring to the molecule upon ionization are restricted to the central benzenic ring.

Table 4 shows the calculated energies for the neutral species (D_{3h} symmetry), the radical cation at the optimized C_{2v} geometries of the A_2 and B_1 states, and the radical cation at the D_{3h} geometry of the neutral species before ionization and at the optimized D_{3h} geometry.

The relaxation from the D_{3h} structure of the neutral molecule to the D_{3h} structure of the ion implies a stabilization energy of 533, 180, and 235 cm^{-1} (ROHF, UB-LYP, and UB3-LYP, respectively). Furthermore, the difference between the energy

TABLE 4: Calculated Energies for Neutral and Radical Cation Species of Triphenylene, and Calculated Stabilization Energies (atomic units)

	RHF/ROHF	UB-LYP	UB3-LYP
neutral D_{3h}	−688.423 1031	−692.728 9616	−693.027 0468
radical cation D_{3h}[a]	−688.158 886 5	−692.470 923 2	−692.754 093 7
radical cation D_{3h}[b]	−688.161 315 0	−692.471 743 5	−692.755 165 9
radical cation C_{2v} (A_2)	−688.165 741 5	−692.473 400 8	−692.757 287 1
radical cation C_{2v} (B_1)	−688.165 606 8	−692.473 453 2	−692.757 332 7
JT Stabilization Energy (cm^{-1}) of C_{2v} Structures			
A_2	972	364	466
B_1	942	375	475

[a] Energy computed at the equilibrium geometry of the neutral molecule [b] Energy computed at the optimized D_{3h} structure of the cation.

of the cation computed at the optimized D_{3h} and C_{2v} structures provides the stabilization due to JT distortion.

It is interesting to compare TPH cation with benzene (BE) cation: theoretical studies on benzene cation show that there are two JT distorted geometries of lower energy.[40] These correspond to elongated and compressed hexagon structures in D_{2h} symmetry. There are three equivalent structures for each of these geometries: three are minima while the other three are saddle points. The calculated average JT stabilization energies for BE cation are 1243, 1061, and 823 cm^{-1} for HF, second-order Moller−Plesset (MP2), and configuration interaction with all single and double excitations (CISD) methods,[40] respectively. A recent detailed study using high-resolution state-to-state threshold photoionization spectroscopy[41] has found that the global minimum geometry is the elongated hexagon (B_{2g} in D_{2h} symmetry), which lies only 8 cm^{-1} below the compressed hexagon (B_{3g} in D_{2h} symmetry).

The average JT stabilization energies we computed for TPH cation with ROHF, UB-LYP, and UB3-LYP calculations (957, 370, and 471 cm^{-1}, respectively) are generally smaller than those calculated for the radical cation of benzene. In order to compare results obtained at equivalent levels of theory, we calculated the energies of the D_{6h} and of the two D_{2h} JT distorted structures of BE cation with the UB-LYP/6-31G method. The computed average JT stabilization energy is 822 cm^{-1}, which confirms a smaller JT stabilization for TPH cation (370 cm^{-1}) compared to BE. Furthermore, the energy difference between the two D_{2h} structures of BE cation is computed to be 8 cm^{-1} which is in surprisingly good agreement with the experimental data.[41] The energy order of the two D_{2h} structures is, however, reversed compared to the experimental conclusions.[41] Nevertheless, the above discussion and comparison with benzene indicates that DFT calculations should give a realistic picture of the energetic of the potential energy surface (PES) of TPH cation.

Turning back to BE cation, the most active vibrational mode which causes the distortion from D_{6h} symmetry is the in-plane ν_6 C−C−C bending. Motion along this coordinate leads to the elongated and compressed hexagonal structures. The zero-point energy of this mode is 413 cm^{-1}, and thus it greatly exceeds the barrier to interconversion of the two JT distorted structures.[41] Therefore, the benzene cation must be viewed as a fluctional system.

Similarly to benzene radical cation, our calculations on TPH radical cation indicate relaxation to two JT distorted geometries belonging to C_{2v} symmetry. The almost negligible energy difference predicted at DFT level of theory for the A_2 and B_1 structures makes the computational determination of the absolute minimum uncertain, in strict analogy with benzene cation. Moreover, the tiny computed energy difference indicates that also TPH cation is a fluxional system, not permanently distorted in one configuration. Rather, the molecule can make excursions over the PES and can visit both C_{2v} structures along the trough of the almost cylindrical potential.

4. Discussion

Vibrational Frequencies of Neutral TPH. Experimental and scaled computed vibrational frequencies for neutral TPH are listed in Table 5. Also shown are scaled calculated frequencies reported by Lifshitz who used the 3-21G basis set.[22] The scaling factors indicated in the table for our calculations are averages of values which bring the experimental and computed frequencies into agreement. Separate scaling factors were determined, one for C−H stretching modes and another for all other modes.

In the D_{3h} point group, the 84 vibrational modes are (10 A_1' + 5 A_1'' + 9 A_2' + 4 A_2'' + 19 E′ + 9 E″), where primed symmetry labels are for in-plane modes, double primed labels for out-of -plane modes, and the E symmetry modes are doubly degenerate. Experimental values listed in the table were determined by Schettino[37] in a study of infrared and Raman spectra of TPH in the crystalline state and in solution. Under the selection rules of this point group, the A_1'' and A_2' fundamentals are inactive in both infrared and Raman spectra for the free molecule. However, molecular distortions in the crystal lower the symmetry so that many forbidden fundamentals are observed in the spectra.

Recently, we discussed some reassignments[10] (italicized frequencies in Table 5) of the fundamentals of TPH on the basis of our simulations of the vibronic activity in the phosphorescence spectrum of the disklike molecule. The scaled calculated vibrational frequencies listed in Table 5 are generally in very good agreement with the experimental values reordered according to the above-mentioned reassignments and confirm the accuracy of our simulated phosphorescence activities in ref 10. Better agreement is found for the DFT methods, B-LYP and B3-LYP, than for HF. This is expected since DFT methods are well-known for good performance in calculating vibrational frequencies.[42] The scaling factors used here primarily account for anharmonicity and electron correlation. Numerical values indicate the degree of overestimation of the correct frequencies. For the neutral TPH data, scaling factors obtained for the three methods are in the range expected.[42] The closest agreement between experimental and calculated frequencies is for the B-LYP (pure DFT method) values of non C−H stretching modes, where the scaling factor is 0.999.

A more thorough comparison between computed and observed fundamentals reveals some discrepancy. The largest differences concern A_2' fundamentals which, among the experimental data, are probably the less secure since they were observed as weak features in the crystal spectra. Given the generally good accuracy of B-LYP/6-31G frequencies, we suspect in particular the bands observed at 1560 and 1422 cm^{-1} in ref 37. An additional discrepancy is found for the band at 1180 cm^{-1} assigned as an A_1' fundamental, which is calculated by the DFT methods to be approximately 30 cm^{-1} higher. This difference is noticeably greater than other observed differences. However, because this was determined to be a polarized Raman band in solution, it must be assigned to the totally symmetric symmetry representation. A large difference occurs also for the band at 152 cm^{-1} assigned as A_2'' because it is the only strong infrared band in this region. The scaled calculated values are all ca. 30 cm^{-1} less, but no other calculated frequencies are reasonably near to this experimental value. Finally, a large difference is computed for the E′ fundamental assigned to the

TABLE 5: Experimental[a] and Scaled Calculated[b] Vibrational Frequencies (cm^{-1}) of Neutral Triphenylene

		6-31G			3-21G			6-31G			3-21G
	expt	HF	B-LYP	B3-LYP	B3-LYP[c]		expt	HF	B-LYP	B3-LYP	B3-LYP[c]
A1′	3055	3090	3077	3078	3096	A2′	3062	3057	3056	3055	3072
	3040	3038	3045	3044	3061		3030	3018	3025	3025	3044
	1550	1545	1553	1554	1555		1560	1610	1605	1613	1604
	1458	1455	1450	1453	1450		1422	1452	1469	1465	1477
	1341	1297	1338	1340	1308		*1320*	1301	1308	1302	1325
	1230	1193	1243	1234	1227		1136	1143	1163	1156	1172
	1180	1139	1210	1202	1209		1025	1012	1011	1008	1032
	1062	1032	1071	1068	1068		607	609	616	612	627
	700	692	702	700	709		550	546	558	555	560
	418	401	414	412	415						
A1″	951	1044	961	976	995	A2″	949	1004	932	946	960
	868	942	858	870	866		741	769	746	748	747
	758	807	766	768	770		422	432	425	425	427
	570	580	571	572	582		152	120	122	121	119
	135	111	112	112							
E′	3085	3088	3074	3075	3093	E″	972	1046	969	983	1000
	3070	3060	3061	3060	3077		936	996	913	929	949
	3038	3035	3041	3040	3058		850	900	851	859	860
	3024	3019	3026	3026	3045		*758*	806	773	777	775
	1611	1614	1598	1608	1599		711	731	708	709	721
	1579	1582	1567	1578	1566		532	555	547	546	539
	1500	1495	1507	1505	1514		432	438	430	430	429
	1434	1434	1450	1444	1460		279	274	271	271	272
	1300	1319	1354	1349	1339			51	55	55	55
	1255	1238	1309	1305	1281						
	1245	1227	1265	1258	1269						
	1167	1167	1196	1186	1211						
	1110	1095	1114	1113	1118						
	1052	1043	1063	1059	1064						
	1003	981	999	998	1006						
	776	765	780	777	786						
	619	625	634	630	643						
	410	397	405	403	408						
	264	251	259	258	261						

[a] Experimental frequencies from ref 37. [b] Two scaling factors are used, one for C−H stretching (RHF = 0.899; B-LYP = 0.974; B3-LYP = 0.947; and another for all other modes (RHF = 0.887; B-LYP = 0.999; B3-LYP = 0.965). [c] From ref 22. Scaling factor for C−H stretching: 0.953; for other modes: 0.976.

1300 cm^{-1} band. In this case, however, the discrepancy is probably due to inaccuracy of the B-LYP (and B3-LYP) calculations in predicting the effects of vibronic coupling on this mode which is dominated by a combination of the ν_{14} of benzene, a mode notoriously sensible to the effects of vibronic coupling.[43] Assignments of the remaining experimental bands fit well to calculated values.

Resonance Raman Spectrum of TPH Radical Cation. According to the structure of the PES of TPH cation predicted by quantum-chemical calculations, the interpretation of the vibronic activity observed in the resonance Raman spectrum would require, in principle, the exact solution of the multimode nonadiabatic JT vibronic problem. The number of JT active vibrations combined with the contribution from TS vibrations makes the problem considerably complex and difficult to solve exactly. Thus, here we adopt a simpler strong-coupling approach,[44] which we employ to evaluate the intensities in the resonance Raman spectrum due to each of the two C_{2v} distorted structures. We believe that the good quality of simulated RR spectra supports this choice and provides a realistic indication of the JT activity in TPH cation. In this model, the adiabatic anharmonic potential due to JT interactions is substituted by a diabatic displaced harmonic potential centered at the JT distorted geometry. The newly defined potential is employed to evaluate the displacement parameters B_i through eq 1.

The B_i parameters were computed for the two JT distorted structures corresponding to the A_2 and B_1 states. To this end, we carried out QCFF/PI + CI calculations to identify the resonant states responsible for the strong absorption at about 400 nm. The CI calculations included all the single excitations arising from the highest five occupied molecular orbitals + the SOMO, to the lowest six unoccupied molecular orbitals, for a total of 102 determinants. The resulting lowest electronic states are listed, along with the $D_0 \rightarrow D_n$ oscillator strengths *f*, in Table 6. To differentiate between the states computed at the geometry of the A_2 state from those computed at the geometry of the B_1 state, we label the second set of states with a prime in Table 6 and in the following. Inspection of the data in Table 6 shows that for both the A_2 and B_1 JT distorted structures of TPH cation a strong transition is predicted at 386 nm, which is assigned to the experimentally observed absorption at 400 nm. The equilibrium geometries of the two resonant excited states D_6 and D_6' were obtained with the same QCFF/PI + CI calculations and are listed in Table 7 along with the geometry difference with respect to the structure of the two C_{2v} states $D_0(A_2)$ and $D_0'(B_1)$.

The computed D_6-D_0 ($D_6'-D_0'$) geometry differences were projected onto the D_0 (D_0') vibrational normal coordinates to obtain the B_i displacement parameters and hence the γ_i parameters which are directly related to the RR activity. Three sets of normal coordinates were employed to produce the γ_i parameters: those obtained from semiempirical QCFF/PI + CI calculations, and two ab initio sets from the ROHF/6-31G and B-LYP/6-31G calculations. The resulting γ_i parameters are listed in Table 8 along with the computed TS vibrational frequencies of the two C_{2v} states of TPH cation. A more appealing

TABLE 6: QCFF/PI Excitation Energies and Oscillator Strengths (*f*) of the Lowest Electronic States of TPH Cation Computed at the Two C_{2v} Structures

	E (eV)	sym	*E* (nm)	*f*
		A_2 Structure[a]		
D_0	0.0000	A_2		
D_1	0.2431	B_1	5100	0.0001
D_2	0.9689	A_2	1280	0.0477
D_3	1.9310	B_1	642	0.0888
D_4	1.9315	A_2	642	0.0331
D_5	2.1081	B_1	588	0.0941
D_6	3.2130	B_1	386	0.1164
		B_1 Structure[b]		
D_0'	0.0000	B_1		
D_1'	0.2290	A_2	5415	0.0007
D_2'	0.9682	A_2	1281	0.0508
D_3'	1.9177	B_1	647	0.0687
D_4'	1.9331	A_2	641	0.0380
D_5'	2.0838	B_1	595	0.1064
D_6'	3.2111	A_2	386	0.1080

[a] QCFF/PI + CI calculations carried out at the A_2 state structure. [b] QCFF/PI + CI calculations carried out at the B_1 state structure.

TABLE 7: Calculated Equilibrium Geometrical Parameters of the Two Excited States D_6 and D_6' in Resonance with the Two C_{2v} States D_0 and D_0' of Triphenylene Radical Cation[a]

	QCFF/PI calculations			
parameters	$D_6(B_1)$	$D_6'(A_2)$	$D_6(B_1)$-$D_0(A_2)$	$D_6'(A_2)$-$D_0'(B_1)$
r(2−3)	1.3800	1.4443	−0.0138	0.0195
r(14−15)	1.4530	1.5183	0.0074	0.0511
r(17−18)	1.4060	1.4890	−0.0278	0.0030
r(3−4)	1.4268	1.3760	0.0224	−0.0058
r(4−15)	1.4282	1.4447	0.0061	0.0084
r(15−16)	1.4595	1.4157	−0.0147	−0.0322
r(16−17)	1.4918	1.4659	0.0294	0.0144
r(8−17)	1.4638	1.4019	0.0151	−0.0093
r(5−16)	1.4160	1.4611	0.0000	0.0213
r(5−6)	1.4000	1.3950	0.0037	0.0021
r(6−7)	1.4249	1.3955	0.0103	−0.0038
r(7−8)	1.3767	1.4279	−0.0043	0.0211
α(2,3,4)	120.12	120.63		
α(3,4,15)	121.46	122.01		
α(4,15,14)	118.41	117.36		
α(14,15,16)	120.07	119.91		
α(15,16,17)	119.54	120.64		
α(16,17,18)	120.39	119.44		
α(8,17,16)	117.25	119.00		
α(5,16,17)	118.26	117.39		
α(6,5,16)	121.99	121.39		
α(5,6,7)	120.41	120.43		
α(6,7,8)	120.53	120.11		
α(7,8,17)	121.56	121.67		

[a] Bond lengths in Å, bond angles in degrees.

representation of the computed activities is depicted in Figures 2 and 3 where the spectra simulated by using QCFF/PI (Figure 2) and B-LYP/6-31G (Figure 3) vibrational coordinates are presented.

Inspection of Table 8 and Figures 2 and 3 shows that, interestingly, the RR activities predicted for the two JT structures (the $D_0(A_2)$ and $D_0'(B_1)$ states) of TPH cation are substantially similar. Moreover, the simulated spectra of Figures 2 and 3 show the strongest activity in frequency regions where bands are correspondingly observed.

In the following we restrict the comparison between observed and computed bands to the spectra simulated using the B-LYP/6-31G normal coordinates and frequencies, since the latter are much closer to observed frequencies. Similar considerations do apply, however, to the simulated spectra produced with all the three sets of normal coordinates, although a less satisfactory agreement was obtained with the use of ROHF/6-31G vibrational coordinates.

In the spectral region examined experimentally (∼400−1600 cm^{-1}), 12 bands are identified. Most experimental frequencies are close to a calculated fundamental of the two C_{2v} structures whose RR activity is predicted to be nonnegligible. The strongest observed band in the RR spectrum (419 cm^{-1}) is assigned to the computed 399 (A_2 state) or 404 (B_1 state) cm^{-1} fundamentals. The following two bands observed at 596 and 683 cm^{-1} are also easily assigned to the computed 613 (A_2 state) cm^{-1}, 623 (B_1 state) cm^{-1}, and 687 cm^{-1} fundamentals. Similarly, the computed 1073 and 1068 cm^{-1} fundamentals match the activity observed at 1062 cm^{-1}. The observed 1103 cm^{-1} band can be assigned to the computed 1110 (A_2 state), 1102 (B_1 state) cm^{-1} fundamentals, although the predicted intensity is very weak. In the 1200−1400 cm^{-1} spectral region, four bands are observed at 1269, 1333, 1365, and 1375 cm^{-1}. In the same region the simulated spectra of Figure 3 show four prominent bands whose intensities reproduce quite closely the experimental spectrum (see also Table 8). Above 1400 cm^{-1}, two clear bands are observed at 1458 and 1553 cm^{-1}. The first is assigned to a medium-weak band predicted at 1452 (A_2 state) or 1453 cm^{-1} (B_1 state) for the two C_{2v} structures. The intensity of this band is underestimated by the calculations. The second band is slightly more difficult to assign, since the simulated spectra show much more activity in this region compared to the experimental spectrum. As will be seen below, the stronger intensity above 1550 cm^{-1} is most probably attributed to an overestimate of the JT activity in this region by the QCFF/PI + CI calculations that were employed to obtain the D_0-D_6 ($D_0'-D_6'$) geometry changes. The band observed at 1553 cm^{-1} is assigned to the medium-intensity band computed at 1556 (A_2 state) or 1544 cm^{-1} (B_1 state). In summary, 11 out of the 12 bands observed in the matrix spectrum are assigned to A_1 fundamentals of the C_{2v} structures. According to the FC mechanism, besides totally symmetric modes, their overtones and combinations, and overtones and combinations of non-totally symmetric modes having even number of vibrational quanta can also appear in the spectrum. Thus, the weak band observed at 834 cm^{-1} in the matrix is assigned to the first overtone of the strong fundamental band located at 419 cm^{-1} in the matrix. Some assignments, other than to fundamentals, would therefore include the following combination bands: 1062 cm^{-1} (419 + 596 cm^{-1} fundamentals), 1103 cm^{-1} (419 + 683 cm^{-1} fundamentals), and 1269 cm^{-1} (596 + 683 cm^{-1} fundamentals). In other words, these three bands in the spectrum assigned as fundamentals may have contributions from combinations. This is likely to be the case especially for the 1103 cm^{-1} band. Although there is one TS frequency in this region, its activity in the RR spectrum is predicted to be almost negligible.

In order to analyze in more detail the nature of the activity in the RR spectrum, we projected the D_0-D_6 ($D_0'-D_6'$) geometry changes over the normal coordinates of the neutral species (D_{3h} symmetry). This enabled us to distinguish between RR active modes related to TS modes in D_{3h} and those related to JT active modes in D_{3h} (E′ symmetry modes). This analysis suggests that 60% of the activity predicted in the RR spectrum is due to modes which correlate with TS modes in D_{3h}. Thus, the activity observed at 683, 1062, 1269, 1365, 1458, and 1553 cm^{-1} is almost entirely due to vibrations that would be TS in D_{3h}. Conversely, clear signatures of JT activity are the 419 and 596 cm^{-1} bands, as well as the congestion of bands observed around 1350 cm^{-1}. In D_{3h} symmetry, in the latter frequency region there are three E′ modes and one TS mode. In C_{2v}

TABLE 8: Experimental and Calculated Totally Symmetric (a_1) Vibrational Frequencies (cm^{-1}) for the Two C_{2v} States $D_0(A_2)$ and $D_0'(B_1)$ of Triphenylene Radical Cation and Calculated Activity (γ Parameters) in the Resonance Raman Spectrum

	QCFF/PI				ROHF/6-31G[b]				UB-LYP/6-31G[b]			
expt[a]	A_2	γ	B_1	γ	A_2	γ	B_1	γ	A_2	γ	B_1	γ
	1581	0.087	1572	0.137	1620	0.079	1588	0.149	1597	0.060	1578	0.111
1553	1548	0.010	1539	0.050	1567	0.023	1551	0.029	1556	0.031	1544	0.044
	1512	0.001	1513	0.006	1523	0.000	1522	0.008	1529	0.001	1529	0.018
	1504	0.006	1493		1495	0.005	1476	0.000	1503	0.003	1496	0.007
1458	1450	0.002	1455	0.009	1448	0.025	1453	0.043	1451	0.008	1452	0.008
	1433	0.017	1442	0.028	1416	0.021	1428	0.009	1448	0.001	1443	0.009
1375	1370	0.023	1368	0.064	1358	0.037	1355	0.133	1364	0.024	1364	0.046
1365	1312	0.037	1308	0.020	1295	0.104	1299	0.061	1340	0.090	1343	0.144
	1275	0.006	1274	0.010	1239	0.050	1260	0.029	1325	0.035	1314	
1333	1281	0.104	1296	0.113	1231	0.005	1230	0.054	1286	0.027	1284	0.024
1269	1241	0.052	1236	0.049	1215	0.013	1212	0.046	1256	0.065	1255	0.078
	1174	0.003	1174		1183	0.007	1187	0.013	1214		1214	
	1162	0.006	1165	0.005	1131	0.017	1173	0.003	1194	0.006	1204	0.008
1103	1095		1092	0.002	1086	0.003	1089	0.000	1110	0.001	1102	
1062	1072	0.019	1074	0.012	1045	0.030	1044	0.024	1073	0.026	1068	0.021
	1053		1039	0.001	1020	0.013	995	0.002	1049	0.004	1035	0.001
	1007	0.001	1004	0.021	979	0.001	953	0.013	984		979	0.017
	775	0.005	775	0.007	758	0.009	758	0.014	770	0.006	776	0.010
683	709	0.072	709	0.107	674	0.049	676	0.085	687	0.058	687	0.088
596	626	0.017	625	0.011	608	0.042	609	0.029	613	0.024	623	0.021
	434	0.020	434	0.019	405	0.009	404	0.006	415	0.018	415	0.005
419	391	0.066	391	0.163	388	0.082	395	0.206	399	0.071	404	0.189
	261	0.005	258	0.025	254	0.004	250	0.019	261	0.004	257	0.018

[a] Experimental frequencies from the cation spectrum in 77 K Freon matrix. An additional band is observed at 834 cm^{-1} which is assigned as the overtone of the 419 cm^{-1} band. (See the discussion in the text.) [b] Scaling factors for ROHF and UB-LYP frequencies of the radical cation are the same as those used for neutral TPH.

symmetry, however, all the above modes are TS and some mixing occurs which distributes the intensity among several bands. We also believe that the large number of TS fundamentals in this region (in C_{2v}) is probably the cause of an unbalanced mixing which leads to the underestimate of the fundamental assigned to the observed 1333 cm^{-1} band (see Table 8). Moreover, in this frequency region most vibrations bear some parentage with the ν_{14} mode of benzene, a mode whose frequency is notoriously difficult to calculate because of vibronic coupling effects.[43] As anticipated, the strong activity above 1550 cm^{-1} predicted by the simulations is most likely an artifact of the calculations. It is known that the QCFF/PI method tends to overestimate vibronic couplings due to CC stretchings. As a consequence the adiabatic potentials corresponding to the JT distorted structures may show artificially enhanced displacements along these CC stretching modes. This explains the strong predicted activity above 1550 cm^{-1} which is mainly due to modes that correlate with E′ modes in D_{3h}.

In conclusion, the RR spectra simulated under the stringent approximation of strong JT coupling account surprisingly well for the bands observed in the matrix spectrum and are a valid support for the assignment of experimentally observed bands.

The strongest JT active modes are the 419 and 596 cm^{-1} bands. Inspection of the molecular motion associated with these two frequencies shows that they are dominated by combinations of the ν_6 of benzene. A graphical representation of the two active modes is shown in Figure 4. The modes in Figure 4 correspond to the B-LYP/6-31G normal coordinates of the A_2 state, but exactly the same shape is found for the corresponding modes of the B_1 state. Since the ν_6 is the most active JT mode of benzene, this is another indication of the close similarity between benzene and TPH cation. Calculations are in progress to evaluate the JT couplings in order to compare the results of the simulations presented here with more exact multimode JT vibronic models.

Because of the fluxionality of TPH cation resulting from this study, we cannot associate the experimentally observed bands

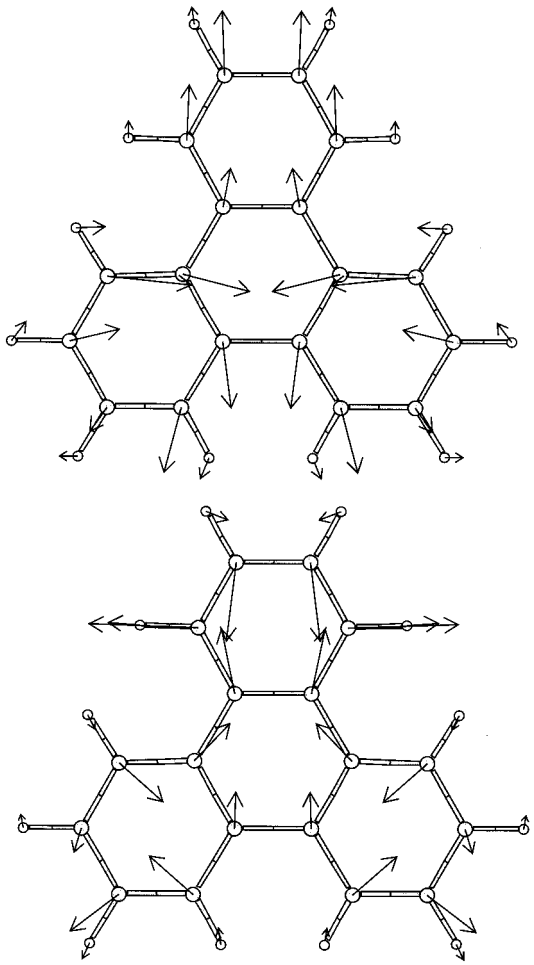

Figure 4. Molecular motion associated with the two active bands in the RR spectrum of TPH cation due to JT active modes: (a, top) mode computed at 415 cm^{-1} (B-LYP/6-31G frequency of the A_2 state); (b, bottom) mode computed at 613 cm^{-1} (B-LYP/6-31G frequency of the A_2 state).

to one of the two locally nondegenerate C_{2v} structures. In this sense, a direct numerical comparison between computed frequencies (belonging to a statically distorted structure) and observed bands (due to the fluctional system) has little meaning. For this reason, the computed TS vibrational frequencies of *both* the A_2 and B_1 states were only used as a guide to assign the observed RR spectrum discussed above.

5. Summary and Conclusions

TPH radical cation has been generated by γ-irradiation in a low-temperature Freon matrix. RR spectra were measured using excitation within the electronic absorption band located near 400 nm. Equilibrium geometries and vibrational frequencies were calculated for both the neutral and radical cation species, using three levels of ab initio theory: HF, B-LYP, and B3-LYP along with semiempirical QCFF/PI + CI calculations. The two JT distorted structures of C_{2v} symmetry were optimized for TPH cation with all the methods above. While QCFF/PI and ROHF predict the A_2 state to be the lowest energy structure, both DFT methods favor the B_1 state. The negligible energy difference between the A_2 and B_1 states indicates, however, that TPH cation, similarly to BE cation is a fluxional system and can make free excursions over the PES.

With the help of quantum-chemical calculations, RR activities were simulated for the two C_{2v} structures and used to assign the observed bands. The combination of experimental and computational results show that the bands observed in the RR spectrum of the radical cation include some signatures clearly indicating the JT activity which distorts dynamically the cation from D_{3h} to C_{2v} symmetry. The most active JT modes are combinations of the ν_6 of benzene and are identified with the observed 419 and 596 cm^{-1} bands in the RR spectrum.

Acknowledgment. We thank J. F. Offersgård for valuable assistance with hardware and software, and Professor Torben Lund for help with purifying the triphenylene samples. This work was supported by a grant from the Danish National Science Research Council to the Center for Molecular Dynamics and Laser Chemistry, from the Italian National Research Council (CNR, Project "Applicazioni di spettroscopie ottiche"), from MURST (Project "Analisi della struttura vibrazionale di spettri elettronici", ex 60%), and from the University of Bologna (Funds for selected research topics: Project "Materiali innovativi").

References and Notes

(1) Etchegoin, P. *Phys. Rev. E* **1997**, *56*, 538.
(2) Adam, D.; Schuhmacher, P.; Simmerer, J.; Haussling, L.; Siemensmeyer, K.; Etzbach, K. H.; Ringsdorf, H.; Haarer, D. *Nature* **1994**, *371*, 141.
(3) Adam, D.; Closs, F.; Frey, T.; Funhoff, D.; Haarer, D.; Ringsdorf, H.; Schuhmacher, P.; Siemensmeyer, K. *Phys. Rev. Lett.* **1993**, *70*, 457.
(4) Closs, F.; Siemensmeyer, K.; Frey, T.; Funhoff, D. *Liq. Cryst.* **1993**, *14*, 629.
(5) Markovitsi, D.; Lecuyer, I.; Lianos, P.; Malthete, J. *J. Chem. Soc., Faraday Trans.* **1991**, *87*, 1785.
(6) Markovitsi, D.; Rigaut, F.; Mouallem, M. *Chem. Phys. Lett.* **1987**, *135*, 236.
(7) Braitbart, O.; Sasson, R.; Weinreb, A. *Mol. Cryst. Liq. Cryst.* **1988**, *159*, 233.
(8) Markovitsi, D.; Germain, A.; Millie, P.; Lecuyer, P.; Gallos, L. K.; Argyrakis, P.; Bengs, H.; Ringsdorf, H. *J. Phys. Chem.* **1995**, *99*, 1005.
(9) Baunsgaard, D.; Larsen, M.; Harrit, N.; Frederiksen, J.; Wilbrandt, R.; Stapelfeldt, H. *J. Chem. Soc., Faraday Trans.* **1997**, *93*, 1893.
(10) Baunsgaard, D.; Harrit, N.; El Balsami, M.; Negri, F.; Orlandi, G.; Frederiksen, J.; Wilbrandt, R. *J. Phys. Chem. A* **1998**, *102*, 10007.
(11) Boden, N.; Bushby, R. J.; Clements, J.; Luo, R. *J. Mater. Chem.* **1995**, *5*, 1741.
(12) Keszthelyi, T.; Wilbrandt, R *J. Phys. Chem.* **1996**, *100*, 15785.
(13) Keszthelyi, T.; Wilbrandt, R.; Bally, T. *J. Phys. Chem.* **1996**, *100*, 16843.
(14) Keszthelyi, T.; Wilbrandt, R.; Bally, T.; Roulin, J.-L. *J. Phys. Chem.* **1996**, *100*, 16850.
(15) Grage, M. M.-L.; Keszthelyi, T.; Offersgaard, J. F.; Wilbrandt, R. *Chem. Phys. Lett.* **1998**, *282*, 171.
(16) Brouwer, A. M.; Langkilde, F. W.; Bajdor, K.; Wilbrandt, R. *Chem. Phys. Lett.* **1994**, *225*, 386.
(17) Brouwer, A. M.; Wilbrandt, R. J. *J. Phys. Chem.* **1996**, *100*, 9678.
(18) Brouwer, A. M.; Wiering, P. G.; Zwier, J. M.; Langkilde, F. W.; Wilbrandt, R. *Acta Chem. Scand.* **1997**, *51*, 217.
(19) Brouwer, A. M.; Zwier, J. M.; Svendsen, C.; Mortensen, O. S.; Langkilde, F. W.; Wilbrandt, R. *J. Am. Chem. Soc.* **1998**, *120*, 3748.
(20) Negri, F.; Orlandi, G. *J. Mol. Struct.* **2000**, *521*, 197.
(21) Negri, F. *Vib. Spectrosc.* **2000**, *24*, 125.
(22) Ling, Y.; Lifshitz, C. *J. Mass Spectrosc.* **1997**, *32*, 1219.
(23) Langhoff, S. *J. Phys. Chem.* **1996**, *100*, 2819.
(24) Torii, H. *Chem. Phys. Lett.* **1999**, *306*, 381.
(25) Becke, A. D. *Phys. Rev. A* **1988**, *38*, 3098.
(26) Lee, C.; Yang, W.; Parr, R. G. *Phys. Rev. B* **1988**, *37*, 785.
(27) Becke, A. D. *J. Chem. Phys.* **1993**, *98*, 5648.
(28) Frisch, M. J.; Trucks, G. W.; Schlegel, H. B.; Scuseria, G. E.; Robb, M. A.; Cheeseman, J. R.; Zakrzewski, V. G.; Montgomery, J. A. Jr.; Stratmann, R. E.; Burant, J. C.; Dapprich, S.; Milla, J. M.; Daniels, A. D.; Kudin, K. N.; Strain, M. C.; Farkas, O.; Tomasi, J.; Barone, V.; Cossi, M.; Cammi, R.; Mennucci, B.; Pomelli, C.; Adamo, C.; Clifford, S.; Ochterski, J.; Petersson, G. A.; Ayala, P. Y.; Cui, Q.; Morkuma, K.; Malick, D. K.; Rabuck, A. D.; Raghavachari, K.; Foresman, J. B.; Cioslowski, J.; Ortiz, J. V.; Stefanov, B. B.; Liu, G.; Liashenko, A.; Piskorz, P.; Komaromi, I.; Gomperts, R.; Martin, R. L.; Fox, D. J.; Keith, T.; Al-Laham, M. A.; Peng, C. Y.; Nanayakkara, A.; Gonzalez, C.; Challacombe, M.; Gill, P. M. W.; Johnson, B. G.; Chen, W.; Wong, M. W.; Andres, J. L.; Gonzalez, C.; Head-Gordon, M.; Replogle, E. S.; Pople, J. A. *Gaussian 98*, Revision A.6; Gaussian, Inc.: Pittsburgh, PA 1998.
(29) Negri, F.; Orlandi, G.; Brouwer, A. M.; Langkilde, F. W.; Wilbrandt, R. *J. Chem. Phys.* **1989**, *90*, 5944.
(30) Negri, F.; Orlandi, G. *J. Phys. B* **1996**, *29*, 5049.
(31) Warshel, A.; Karplus, M. *J. Am. Chem. Soc.* **1972**, *92*, 5612.
(32) Armstrong, D. R.; Fortune, R.; Perkins, P. G.; Stewart, J. J. P. *J. Chem. Soc., Faraday Trans. 1* **1972**, *68*, 1839.
(33) Morton, J. R.; Negri, F,; Preston, K. F. *Can. J. Chem.* **1994**, *72*, 776.
(34) Langkilde, F. W.; Bajdor, K.; Wilbrandt, R.; Negri, F.; Zerbetto, F.; Orlandi, G. *J. Chem. Phys.* **1994**, *100*, 3503.
(35) Albrecht, A. C. *J. Chem. Phys.* **1961**, *34*, 1476.
(36) Shida, T. *Electronic Absorption Spectra of Radical Ions;* Physical Sciences Data 34; Elsevier: Amsterdam, 1988.
(37) Schettino, V. *J. Mol. Spectrosc.* **1970**, *34*, 78.
(38) Ahmed, F. R.; Trotter, J. *Acta Crystallogr.* **1963**, *16*, 503.
(39) Keszthelyi, T.; Grage, M. M.-L.; Offersgaard, J. F.; Wilbrandt, R.; Svendsen, C.; Mortensen, O. S.; Pedersen, J. K.; Jensen, H. J. Aa. *J. Phys. Chem.*, submitted for publication.
(40) Raghavachari, K.; Haddon, R. C.; Miller, T. A.; Bondybey, V. E. *J. Chem. Phys.* **1983**, *79*, 1387.
(41) Lindner, R.; Muller-Dethlefs, K.; Wedum, E.; Haber, K.; Grant, E. R. *Science* **1996**, *271*, 1698.
(42) Scott, A. P.; Radom, L. *J. Phys. Chem.* **1996**, *100*, 16502.
(43) Negri, F.; Orlandi, G. *J. Raman Spectrosc.* **1998,** *29*, 501.
(44) Henneker, W. H.; Penner, A. P.; Siebrand, W.; Zgierski, M. Z. *J. Chem. Phys.* **1978**, *69*, 1884.